ISSN 0915-633X

NATIONAL INSTITUTE FOR FUSION SCIENCE

MHD-Vlasov Simulation of the Toroidal Alfvén Eigenmode

Y. Todo, T. Sato, K. Watanabe, T.H. Watanabe and R. Horiuchi

(Received - Oct. 28, 1994)

NIFS-319 Nov. 1994

RESEARCH REPORT
NIFS Series

NAGOYA, JAPAN

MHD-Vlasov Simulation of the Toroidal Alfvén Eigenmode

Y. Todo, T. Sato, K. Watanabe, T. H. Watanabe, and R. Horiuchi

Theory and Computer Simulation Center

National Institute for Fusion Science, Chikusa-ku, Nagoya 464-01, Japan

Abstract

A new simulation method has been developed to investigate the excitation and saturation processes of toroidal Alfvén eigenmodes (TAE modes). The background plasma is described by a full-MHD fluid model, while the kinetic evolution of energetic alpha particles is followed by the drift kinetic equation. The magnetic fluctuation of $n = 2$ mode develops and saturates at the level of 1.8×10^{-3} of the equilibrium field when the initial beta of alpha particles is 2% at the magnetic axis. After saturation, the TAE mode amplitude shows an oscillatory behavior with a frequency corresponding to the bounce frequency of the alpha particles trapped by the TAE mode. The decrease of the power transfer rate from the alpha particles to the TAE mode, which is due to the trapped particle effect of a finite-amplitude wave, causes the saturation. From the linear growth rate the saturation level can be estimated.

Keywords: toroidal Alfvén eigenmode, alpha particles, MHD-Vlasov simulation, nonlinear Landau damping, particle trapping

1. Introduction

The toroidal Alfvén eigenmode (TAE mode)[1] has recently become the focus of attention for fusion physicists, since it can be excited resonantly with alpha particles of 3.52 MeV which are produced from deuterium-tritium reactions. TAE modes are destabilized when the alpha particle distribution has a density gradient. Fu and Van Dam[2] studied the linear stability of TAE mode with alpha particles in terms of a linearized drift kinetic equation, and found that there are two conditions for the TAE mode to be unstable. The first condition requires that the scale length of the alpha particle density gradient is sufficiently small. The second condition requires that the alpha particle destabilization effects overcome the electron Landau damping effect.

One of the unresolved, but significant problems of the TAE mode is the saturation mechanism and the saturation level. Sigmar *et al.*[3] analyzed alpha particle losses using a Hamiltonian guiding center code for a given linear TAE mode, and found that for the amplitude of $\tilde{B}_r/B_0 \geq 10^{-3}$, a substantial fraction of alpha particles can be lost in one slowing down time. This indicates that a precise knowledge of the saturation level and the saturation mechanism is crucial for ignited tokamak plasmas. Breizman *et al.*[4] discussed the saturation level in the context of the nonlinear Landau damping which is studied by O'Neil[5] . Wu and White[6] studied the saturation calculating the nonlinear alpha particle dynamics with a linear TAE mode which evolves with the linear dispersion relation obtained by the linear analysis based on the alpha particle distribution. They found that modification of the particle distribution leads to mode saturation.

Computer simulation is a powerful tool to elucidate the saturation mechanism

of TAE mode. Spong *et al.*[7,8] carried out linear and nonlinear simulations in which the background plasma is described by a reduced MHD fluid model and the alpha particles by a gyrofluid model. They argue that the saturation occurs due to the nonlinearly enhanced continuum damping and the nonlinearly generated $\mathbf{E}\times\mathbf{B}$ flows. In their work, alpha particles are represented only by two components, namely, the density and the parallel flow velocity. Therefore, their method could not analyze the kinetic effects of the finite-amplitude TAE mode on the alpha particles which are the energy source for the mode. Park *et al.*[9] developed another simulation technique in which they make use of an MHD fluid model and super particles as the energetic particles. Their method seems to suffer numerical noises which unavoidably arise because of a limited number of super particles, though it contains kinetic characters of alpha particles.

We have developed a new simulation method that enables us to investigate excitation and saturation of toroidal Alfvén eigenmodes. In this method, the background plasma is described as a full-MHD fluid, while the kinetic evolution of the energetic alpha particles is followed by the drift kinetic equation. Both the MHD and drift kinetic equations are solved by a finite difference method. This new method can deal with the kinetic characters of alpha particles with nonlinear MHD waves free from numerical noises of particle discreteness.

In the present paper, we study the excitation and saturation process of the TAE mode using the new simulation method mentioned above. We focus particularly on the $n = 2$ TAE mode and its nonlinear evolution including the generation of the $n = 0$ mode. The plasma model and the simulation method are presented in section 2. In section 3 we present the simulation results, comparing with the linear theory, and discuss on the saturation mechanism. We analyze the power transfer rate and

show that the decrease of the rate causes the saturation of the instability. We show that the saturation is caused by the trapped particle effect of the finite-amplitude wave. Finally, a conclusion is given in section 4.

2. Simulation model

In our model, the background plasma is described by the ideal MHD equations and the electric field is given by the MHD description which is a reasonable approximation under the condition that the alpha density is much less than the background plasma density:

$$\frac{\partial \rho}{\partial t} = -\nabla \cdot (\rho \mathbf{v}), \tag{1}$$

$$\rho \frac{\partial}{\partial t}\mathbf{v} + \rho \mathbf{v} \cdot \nabla \mathbf{v} = -\nabla p + \tfrac{1}{\mu_0}(\nabla \times \mathbf{B}) \times \mathbf{B}, \tag{2}$$

$$\frac{\partial \mathbf{B}}{\partial t} = -\nabla \times \mathbf{E}, \tag{3}$$

$$\frac{\partial p}{\partial t} = -\nabla \cdot (p\mathbf{v}) - (\gamma - 1) p \nabla \cdot \mathbf{v}, \tag{4}$$

$$\mathbf{E} = -\mathbf{v} \times \mathbf{B}, \tag{5}$$

where μ_0 is the vacuum magnetic permeability and γ is the adiabatic constant, and all other quantities are conventional.

The energetic alpha particles are described by the drift kinetic equation constructed with the following equation of motion of an alpha particle under the guiding-center approximation with the $\mathbf{E} \times \mathbf{B}$, grad-B, and curvature drifts

$$\frac{d}{dt}\mathbf{x} = \mathbf{v}_{\parallel} + \mathbf{v}_E + \mathbf{v}_d, \tag{6}$$

$$\frac{d}{dt}\epsilon = e_\alpha \mathbf{v}_d \cdot \mathbf{E} + \mu \frac{\partial}{\partial t} B, \tag{7}$$

$$\epsilon = \frac{1}{2}m_\alpha v_\parallel^2 + \mu B, \tag{8}$$

$$\mu = const., \tag{9}$$

$$\mathbf{v}_E = \frac{\mathbf{E}\times\mathbf{B}}{B^2}, \tag{10}$$

$$\mathbf{v}_d = \frac{m_\alpha}{e_\alpha B}(v_\parallel^2\kappa - \frac{\mu}{m_\alpha}\frac{\partial}{\partial\mathbf{x}}B)\times\mathbf{b}, \tag{11}$$

where $v_\parallel$ is the velocity parallel to the magnetic field, μ is the magnetic moment which is the adiabatic invariant, and κ is the magnetic curvature vector. From Eqs. (6)-(11) we can obtain the drift kinetic equation which describes the temporal evolution of the alpha distribution function in the phase space $(\mathbf{x}, v_\parallel, \mu)$:

$$\frac{\partial}{\partial t}f(\mathbf{x}, v_\parallel, \mu) = -\frac{\partial}{\partial\mathbf{x}}[(\mathbf{v}_\parallel + \mathbf{v}_E + \mathbf{v}_d)f] - \frac{\partial}{\partial\mathbf{v}_\parallel}(\mathbf{a}f), \tag{12}$$

$$\mathbf{a} = (\frac{e_\alpha}{m_\alpha v_\parallel}\mathbf{v}_d\cdot\mathbf{E} - \frac{\mu}{m_\alpha}\frac{\partial}{\partial\mathbf{x}_\parallel}B)\mathbf{b}. \tag{13}$$

To complete the equation system in a self-contained way, we should take account of the effects of the alpha particles on the background plasma. For this purpose, we invoke the Maxwell equation for the perpendicular component of the electric field:

$$\frac{\partial}{\partial t}\mathbf{E}_\perp = c^2\nabla\times\mathbf{B} - \frac{c^2}{v_A^2}\frac{d}{dt}\mathbf{E}_\perp - \frac{\nabla p\times\mathbf{B}}{\epsilon_0 B^2} - \frac{1}{\epsilon_0}\mathbf{j}_\alpha, \tag{14}$$

$$\frac{d}{dt}\mathbf{E}_\perp \equiv (\frac{\partial}{\partial t} + \mathbf{v}_E\cdot\nabla)\mathbf{E}_\perp, \tag{15}$$

where, in Eq. (14), the second and third terms are the polarization current and the diamagnetic current of the background plasma, respectively, and the fourth term is the current of alpha particles. The polarization current of alpha particles is negligible since the alpha density is much less than the background plasma density. Neglecting the displacement current and multiplying Eq. (14) by $\mathbf{B}$, we obtain the following equation:

$$\rho\frac{d}{dt}\mathbf{E}_\perp\times\frac{\mathbf{B}}{B^2} = (\frac{1}{\mu_0}\nabla\times\mathbf{B} - \mathbf{j}_\alpha)\times\mathbf{B} - \nabla p. \tag{16}$$

We finally arrive at the magnetohydrodynamic momentum equation by approximating the left-hand-side of Eq. (16) by $\rho\frac{d}{dt}\mathbf{v}_E$, since $\rho\mathbf{E}_\perp \times \frac{d}{dt}(\mathbf{B}/B^2)$ is the second order term in the ordering of $E/v_A \ll B$ and $\delta B \ll B$,

$$\rho\frac{\partial}{\partial t}\mathbf{v} + \rho\mathbf{v}\cdot\nabla\mathbf{v} = (\tfrac{1}{\mu_0}\nabla\times\mathbf{B} - \mathbf{j}_\alpha)\times\mathbf{B} - \nabla p, \tag{17}$$

where $\mathbf{v}_E$ is rewritten as $\mathbf{v}$. This relation is nothing but the MHD momentum equation in which the contribution of the alpha particle current is extracted from the total current. This relation is essentially the same as the model of Park *et al.*[9] except for $-e_\alpha n_\alpha \mathbf{E}$ in their force term, though their derivation is different from ours.

We consider the alpha particle current as the sum of the parallel current, the magnetic drift current, and the diamagnetic current:

$$\begin{aligned}
\mathbf{j}_\alpha &= \mathbf{j}_\parallel + \mathbf{j}_d + \mathbf{j}_{diamag} \\
&= \int v_\parallel \mathbf{b} f d^3v + \int \mathbf{v}_d f d^3v - \nabla\times\mathbf{M}, &(18)\\
\mathbf{M} &= \int \mu \mathbf{b} f d^3v. &(19)
\end{aligned}$$

We can easily show that the total energy is conserved in our model. The temporal evolutions of energy for MHD part and alpha particles are, respectively, given by

$$\begin{aligned}
\frac{\partial}{\partial t}E_{\rm MHD} &= -\nabla\cdot\mathbf{F}_{\rm MHD} + \mathbf{v}\cdot(-\mathbf{j}_\alpha\times\mathbf{B}) \\
&= -\nabla\cdot\mathbf{F}_{\rm MHD} - \mathbf{j}_d\cdot\mathbf{E} + \mathbf{E}\cdot\nabla\times\mathbf{M}, &(20)\\
\frac{\partial}{\partial t}E_\alpha &= -\nabla\cdot\mathbf{F}_\alpha + \mathbf{j}_d\cdot\mathbf{E} + \mathbf{M}\cdot\frac{\partial}{\partial t}\mathbf{B}, &(21)\\
\mathbf{F}_{\rm MHD} &= (\frac{1}{2}\rho\mathbf{v}^2 + \frac{\gamma p}{\gamma-1})\mathbf{v} + \frac{1}{\mu_0}\mathbf{E}\times\mathbf{B}, &(22)\\
\mathbf{F}_\alpha &= \int \epsilon(\mathbf{v}_\parallel + \mathbf{v}_E + \mathbf{v}_d) d^3v. &(23)
\end{aligned}$$

We sum these equations using the Maxwell equation $\frac{\partial}{\partial t}\mathbf{B} = -\nabla\times\mathbf{E}$ and a vector identity, and obtain the temporal evolution of the total energy in the following

conservative form:

$$\begin{aligned} \frac{\partial}{\partial t}E_{\rm total} &= \frac{\partial}{\partial t}E_{\rm MHD} + \frac{\partial}{\partial t}E_{\alpha}, \\ &= -\nabla\cdot(\mathbf{F}_{\rm MHD} + \mathbf{F}_{\alpha} + \mathbf{E}\times\mathbf{M}). \end{aligned} \tag{24}$$

In the remainder of the paper, we set the magnetic moments of alpha particles to zero. We solve these equations using a finite difference method of second-order accuracy both in time and in space.

The aspect ratio of the system is 3 and the poloidal cross section is rectangular. The cylindrical coordinate system (R, φ, z) is used. The simulation region is $2a \leq R \leq 4a$, $-a \leq z \leq a$ where a is the minor radius. The simulation region in the φ direction is $0 \leq \varphi \leq \pi$, since we focus on the $n = 2$ TAE mode and its nonlinear evolution. We make use of (65, 20, 65, 60) grid points for $(R, \varphi, z, v_{\|})$ coordinates, respectively. The simulation region in the $v_{\|}$ direction is $-3v_A \leq v_{\|} \leq 3v_A$ with the grid size of $0.1v_A$.

The initial condition is an MHD equilibrium where both the background plasma beta and the plasma beta of alpha particles are 2% at the magnetic axis. We obtain the initial condition using an iterative method. As an initial guess for the iteration, we numerically solved the Grad-Shafranov equation neglecting the alpha particle current, and set the parallel pressure distribution of alpha particles to be proportional to the MHD pressure with a Maxwellian distribution whose thermal velocity $v_{\alpha} \equiv (T_{\alpha}/m_{\alpha})^{1/2}$ is equal to the Alfvén velocity at the magnetic axis. We obtain an exact equilibrium by the iteration both for the MHD force balance and the distribution function of the alpha particles. The magnetic axis locates at $R = R_0 \equiv 3.16a$, $z = 0$.

We show, in Fig. 1, the initial q-profile and the continuous spectrum of two-

mode-coupling model[1,2] of $(n = 2, m = 2)$- and $(n = 2, m = 3)$- modes as functions of the minor radius. The q-value is an average, since the magnetic surface is not a concentric circle. The continuous spectrum is obtained assuming concentric circular magnetic flux surfaces, expanding the toroidicity effect to first order in the inverse aspect ratio a/R. The $q = (2m + 1)/2n = 5/4$ surface is located at $r = 0.35a$ on average. The scale length of the alpha particle pressure gradient at the $q = (2m + 1)/2n$ surface, which is denoted as L, is $0.42a$. The parallel Larmor radius of alpha particles, which is denoted as ρ_α, is set to $a/16$, which leads to the drift frequency of alpha particles at the $q = (2m + 1)/2n$ surface,

$$\begin{aligned} \omega_{*,\alpha} &\equiv \frac{nq\rho_\alpha v_\alpha}{2rL} \\ &= 1.67\omega_A, \end{aligned} \tag{25}$$

where $\omega_A = v_A/R_0$ and v_A is hereafter the Alfvén velocity at the magnetic axis.

3. TAE instability

A. Linear growth

We continued a simulation run up to $t = 1294\omega_A^{-1}$. The TAE mode which consists mainly of $(n = 2, m = 2)$- and $(n = 2, m = 3)$- modes appeared. Shown in Fig. 2 are the toroidal electric field and the alpha particle distribution function at $v_\parallel = -1.05v_A$, $1.05v_A$, and $2.05v_A$ on a poloidal cross section at $t = 423\omega_A^{-1}$ from which the initial one is subtracted. According to the linear theory of TAE, the q-value for coupling of $(n = 2, m = 2)$- and $(n = 2, m = 3)$- modes is $q = 5/4$. It is to be noted that its amplitude is peaked near the $q = 5/4$ surface. For the distribution function, the $m = 3$ component is dominant for $v_\parallel = -1.05v_A$ whereas

the $m = 2$ component is conspicuous for $v_{\|} = 1.05 v_A$. At the $q = 5/4$ surface the phase velocities of the $m = 2$ and $m = 3$ modes have the same absolute value ($= v_A$) with an opposite sign to each other. Thus when $m = 3$ mode has a phase velocity of $-v_A$, $m = 2$ mode has that of v_A, and they interact with alpha particles at each phase velocity.

In Fig. 3, we plot the temporal evolution of $(n = 2, m = 3)$-mode at $r = 0.35a$ where the mode structure is peaked. It is seen that the instability saturates at $t = 640\omega_A^{-1}$. The real frequency is $0.32\omega_A$ and the linear growth rate is $8.8 \times 10^{-3}\omega_A$. After saturation the mode executes an amplitude oscillation.

Let us compare the simulation results with the analytical formula for the linear growth rate based on a localized analysis which is given by Fu and Van Dam[2]

$$\frac{\gamma_L}{\omega_0} \simeq \frac{9}{4}\beta_\alpha\left(\frac{\omega_{*,\alpha}}{\omega_0} - \frac{1}{2}\right)x(1 + 2x^2 + 2x^4)e^{-x^2}, \tag{26}$$

where $x = v_A/\sqrt{2}v_\alpha$ and ω_0 is the real frequency of the TAE mode.

This formula is applicable for alpha particles which have an isotropic Maxwellian distribution. For the distribution with only the parallel velocity component as considered here, the formula is reduced to

$$\frac{\gamma_L}{\omega_0} \simeq \frac{9}{4}\beta_\alpha\left(\frac{\omega_{*,\alpha}}{\omega_0} - \frac{1}{2}\right)2x^5e^{-x^2}. \tag{27}$$

This formula yields the growth rate of $1.10 \times 10^{-2}\omega_A$ for $x = 1/\sqrt{2}$, $\omega_{*,\alpha} = 1.67\omega_A$, and $\beta_\alpha = 1.5\%$ at the $q = 5/4$ surface which coincides within a factor of 1.25, with the rate obtained from our simulation results.

B. Saturation level and mechanism

When the instability growth stops at $t = 640\omega_A^{-1}$, the maximum value of the fluctuating magnetic field becomes 1.8×10^{-3} of the equilibrium field. This value is

significantly large and thus a significant loss of alpha particles may be anticipated[3].

Let us now consider the saturation mechanism. There are two possibilities for saturation mechanisms: (a) mode coupling effects in the MHD component which include generation of $\mathbf{E} \times \mathbf{B}$ flows and enhanced continuum damping[8] ; and (b) effects of finite-amplitude waves on the alpha particles[4] . In order to identify the saturation mechanism we analyze the temporal evolution of the power transfer rate from alpha particles to the MHD component, namely, $< -\mathbf{j}_\alpha \cdot \mathbf{E} >$ ($<>$ means volume integration). We show the temporal evolution of the TAE mode energy in Fig. 4a and the ratio of the power transfer rate to the TAE mode energy (divided by a factor of 2 to relate directly to the growth rate) in Fig. 4b . The ratio fluctuates at the early stage of the simulation since the initial perturbation is not an eigenfunction but an arbitrary one, and it gradually converges to a constant value during the linear growth stage. At $t = 470\omega_A^{-1}$ the ratio begins to decrease, thus leading to saturation of the instability. It is evident that the decrease of the power transfer rate is the cause of the saturation.

After saturation both the TAE mode energy and the power transfer rate show oscillatory behaviors. Specifically, when the ratio becomes above zero at $t = 1010\omega_A^{-1}$ the mode energy begins to increase and when the ratio becomes negative at $t = 1180\omega_A^{-1}$ the mode energy begins to decrease. We have confirmed that the oscillation of the power transfer rate is caused by the evolution of the phase between $\mathbf{j}_\alpha$ and $\mathbf{E}$.

It is well known that resonant particles *in the nonlinear phase of Landau damping* are trapped by the potential well and execute a bounce motion in it[5] . The bounce frequency for the electrostatic Landau damping is given by

$$\omega_b = (eEk/m)^{1/2}. \tag{28}$$

For the TAE mode, the acceleration of a particle by the electric field is different

from the case of the electrostatic Landau damping and is given by the first term of the right-hand-side of Eq. (13). Therefore, the bounce frequency for the alpha-TAE interaction is

$$\begin{aligned} \omega_b &= (e_\alpha v_d E k_\parallel / m_\alpha v_\parallel)^{1/2} \\ &\sim (E k_\parallel v_\parallel / R_0 B)^{1/2}, \end{aligned} \tag{29}$$

where v_d is approximated by $m_\alpha v_\parallel^2 / e_\alpha R_0 B$.

At saturation, the maximum value of the electric field becomes as large as $1.3 \times 10^{-3} v_A B$. This gives the bounce frequency as $\omega_b = 2.2 \times 10^{-2} \omega_A$ at the $q = 5/4$ surface with $v_\parallel = v_A$. The frequency of the oscillation of the TAE mode energy and the power transfer rate in Fig. 4, $\omega_{\rm os}$, is $1.9 \times 10^{-2} \omega_A$. It should be remarked here that ω_b and $\omega_{\rm os}$ coincide with each other. This remarkable coincidence indicates that the oscillation observed is caused by the bounce motion of the particles trapped by the TAE mode. Furthermore, the growth rate $\gamma_L = 8.8 \times 10^{-3} \omega_A$ also coincides fairly well with ω_b and $\omega_{\rm os}$. This coincidence among ω_b, $\omega_{\rm os}$, and γ_L suggests that the instability saturates in the manner of the nonlinear Landau damping of a finite-amplitude wave which is as suggested by O'Neil[5] .

Furthermore, we can estimate the saturation level by the linear growth rate γ_L using the condition ω_b at saturation equals to $\lambda \gamma_L$ where λ is a factor of $\sim O(1)$ and for the present results $\lambda = 2.5$. Making use of Eq. (29) we obtain the saturation level,

$$\delta B \sim E / v_A = \lambda^2 (\frac{\gamma_L}{\omega_A})^2 \frac{2m+1}{n} B. \tag{30}$$

C. Distribution function at the final stage

In Fig. 5 plotted are the same quantities as Fig. 2 but for $t = 1294 \omega_A^{-1}$. Compar-

ing it with Fig. 2, the distribution function shows a very different structure, while the toroidal electric field is still similar. The $(n = 0, m = 0)$ quasi-linear modes are generated through the nonlinear coupling of the $n = 2$ TAE mode and the $n = 2$ modes of the distribution function, and they have become dominant at $t = 1294\omega_A^{-1}$. The quasi-linear modes are the manifestations of the transport of alpha particles by the TAE modes which smoothes the spatial gradient of alpha particle distribution. Though the amplitude of the quasi-linear mode at $t = 1294\omega_A^{-1}$ is a few percent of the initial distribution at $v_\parallel = 0$ at the magnetic axis, it affects the spatial gradient significantly. Fig. 6 shows distributions of alpha particles at $v_\parallel = -1.05v_A$ and $z = 0$ as a function of R which are averaged in the φ-direction at $t = 0$ and $t = 1294\omega_A^{-1}$, respectively. The spatial gradient of the distribution function is reduced to half near $R = 2.8a$ and $3.3a$.

The resonance between the TAE mode and the alpha particles is complicated since the resonance velocity is different for each magnetic surface and the orbit of an alpha particle deviates from a magnetic surface. Though it is difficult to know the details of the resonance, we show in Fig. 7 the distribution function integrated over the volume subtracting the initial one. We can see in Fig. 7 that the number of alpha particles of $-1.7v_A \leq v_\parallel \leq -v_A$, $1.6v_A \leq v_\parallel \leq 2.6v_A$ decreased, and the number for the other parts increased. The absolute value of the change of the distribution function is at most 5.5×10^{-4} of the initial distribution at $v_\parallel = 0$ integrated over the volume.

4. Conclusion

A new simulation method has been developed to investigate the excitation and saturation processes of the TAE modes. In this method, the background plasma

is described by the full-MHD model, while the kinetic evolution of energetic alpha particles is represented by the drift kinetic equation. It is demonstrated that the $n = 2$ TAE mode is excited, the linear growth rate of which is in good agreement with the linear theory of Fu and Van Dam.[2] After saturation the mode amplitude shows an oscillatory behavior with the bounce frequency of alpha particles trapped by the TAE mode. Moreover, the bounce frequency is in agreement with the linear growth rate. The saturation is caused by the decrease of the power transfer rate from alpha particles to the TAE mode. Thus, we conclude that the growth of the unstable mode is suppressed by the trapped particle effect of a finite-amplitude wave.

The saturation of the magnetic field fluctuation can reach to a significant level, e.g. 1.8×10^{-3} of the equilibrium field intensity when the initial beta of alpha particles is 2% at the magnetic axis, which is supposed to lead to a non-negligible alpha particle loss in one slowing time.[3] We can estimate the saturation level by the linear growth rate γ_L using the saturation condition $\omega_b = \lambda\gamma_L$ where λ is a factor of $\sim O(1)$ and for the present results $\lambda = 2.5$,

$$\delta B \sim E/v_A = \lambda^2(\frac{\gamma_L}{\omega_A})^2\frac{2m+1}{n}B.$$

The $(n = 0, m = 0)$ quasi-linear mode of the alpha particle distribution is generated through the nonlinear coupling of the $n = 2$ TAE mode and the $n = 2$ mode of alpha particle distribution. This quasi-linear mode spatially flattens the distribution function, reducing the free energy source of the instability.

This new simulation technique will be useful to study other fast particle physics such as the fishbone and sawtooth oscillations.

Acknowledgments

The authors would like to express their gratitude to Dr. T. Hayashi, Dr. A. Kageyama, and Mr. H. Takamaru for helpful discussions. One of the authors (Y.T.) thanks Dr. N. Nakajima and Dr. H. Sugama for useful comments. Numerical computations are performed at the NIFS Advanced Computing System for Complexity Simulation. This work is partially supported by three Grants-in-Aid of the Ministry of Education, Science and Culture (No. 05836038, No. 06044238, and No. 06858052).

References

[1] C. Z. Cheng and M. S. Chance, Phys.Fluids **29**, 3659 (1986).

[2] G. Y. Fu and J. W. Van Dam, Phys. Fluids **B1**, 1949 (1989).

[3] D. J. Sigmar, C. T. Hsu, R. White, and C. Z. Cheng, Phys. Fluids **B4**, 1506 (1992).

[4] B. N. Breizman, H. L. Berk, and H. Ye, Phys. Fluids **B5**, 3217 (1993).

[5] T. O'Neil, Phys. Fluids **8**, 2255 (1965).

[6] Y. Wu and R. B. White, Phys. Plasmas **1**, 2733 (1994).

[7] D. A. Spong, B. A. Carreras, and C. L. Hedrick, Phys. Fluids **B4**, 3316 (1992).

[8] D. A. Spong, B. A. Carreras, and C. L. Hedrick, Phys. Plasmas **1**, 1503 (1994).

[9] W. Park, S. Parker, H. Biglari, M. Chance, L. Chen, C. Z. Cheng, T. S. Hahm, W. W. Lee, R. Kulsrud, D. Monticello, L. Sugiyama, and R. White, Phys. Fluids **B4**, 2033 (1992).

Figure Captions

FIG. 1. The q-profile and the toroidal shear Alfvén continuous spectrum of the two-mode-coupling model[1,2] for $(n = 2, m = 2)$- and $(n = 2, m = 3)$-modes as functions of the minor radius. The q-value is an average, since the magnetic surface is not a concentric circle. The continuous spectrum is obtained assuming concentric circular magnetic flux surfaces, expanding the toroidicity effect to first order in the inverse aspect ratio a/R.

FIG. 2. a) Contours of E_φ; contours of the alpha particle distribution function subtracting the initial one b) at $v_\parallel = -1.05 v_A$, c) at $v_\parallel = 1.05 v_A$, and d) at $v_\parallel = 2.05 v_A$ on a poloidal cross section $(2a \leq R \leq 4a,\ -a \leq z \leq a)$ at $t = 423 \omega_A^{-1}$ which are normalized by the initial one at $v_\parallel = 0$ at the magnetic axis. Solid curves are for positive values and dashed curves are for negative values. For the TAE mode, the $m = 2$ mode has a large amplitude in the inner part, whereas the $m = 3$ mode is dominant in the outer part.

FIG. 3. Temporal evolution of the $(n = 2, m = 3)$-mode on the $r = 0.35a$ magnetic surface. The real part is plotted in a), and the amplitude is in b).

FIG. 4. Temporal evolutions of a) the TAE mode energy, and b) the ratio of the power transfer rate $< -\mathbf{j}_\alpha \cdot \mathbf{E} >$ to the TAE mode energy, which is divided by a factor of 2 to relate directly to the growth rate. The decrease of this ratio leads to the saturation of the TAE instability.

FIG. 5. a) Contours of E_φ; contours of the alpha particle distribution function subtracting the initial one b) at $v_{||} = -1.05v_A$, c) at $v_{||} = 1.05v_A$, and d) at $v_{||} = 2.05v_A$ on a poloidal cross section ($2a \leq R \leq 4a$, $-a \leq z \leq a$) at $t = 1294\omega_A^{-1}$ which are normalized by the initial one at $v_{||} = 0$ at the magnetic axis. Solid curves are for positive values and dashed curves are for negative values. The TAE mode has the same structure as the linear growth stage in Fig. 2, while the alpha particle distribution function is dominated by the $(n = 0, m = 0)$- quasi-linear modes.

FIG. 6. The alpha particle distribution functions $f(R)$ at $v_{||} = -1.05v_A$ and $z = 0$ which are averaged in the φ-direction and normalized by $f(v_{||} = 0, t = 0)$ at the magnetic axis.

FIG. 7. The alpha particle distribution function $f(v_{||})$ at $t = 1294\omega_A^{-1}$ integrated in the volume subtracting $f(v_{||}, t = 0)$, which is normalized by $< f(v_{||} = 0, t = 0) >$.

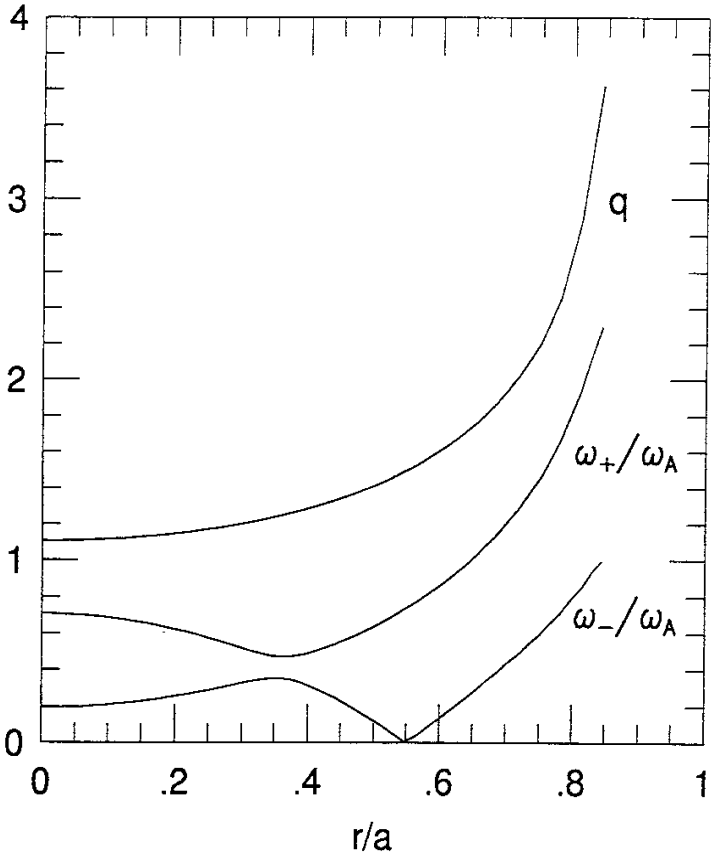

Fig. 1

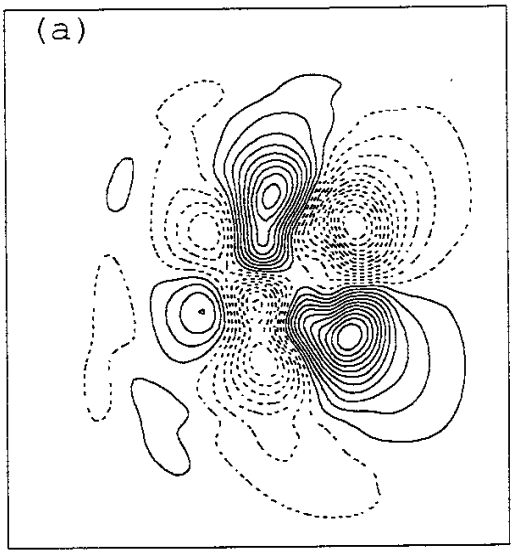

MAX= 3.572E-05 MIN=-3.798E-05

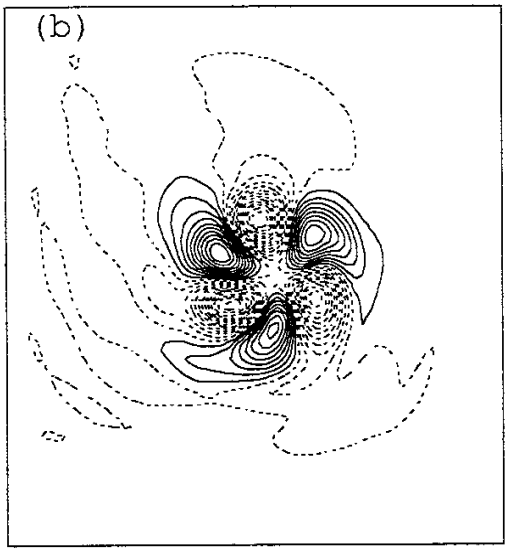

MAX= 2.003E-02 MIN=-2.387E-02

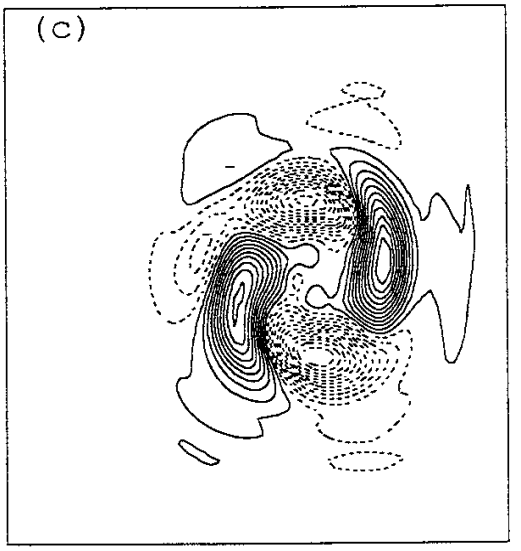

MAX= 6.459E-03 MIN=-7.094E-03

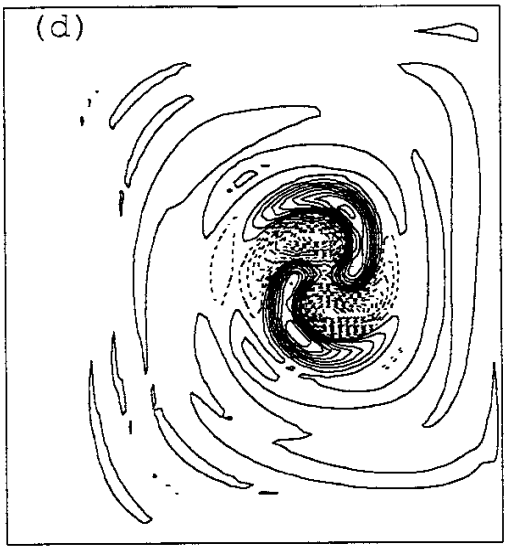

MAX= 4.134E-03 MIN=-6.778E-03

Fig. 2

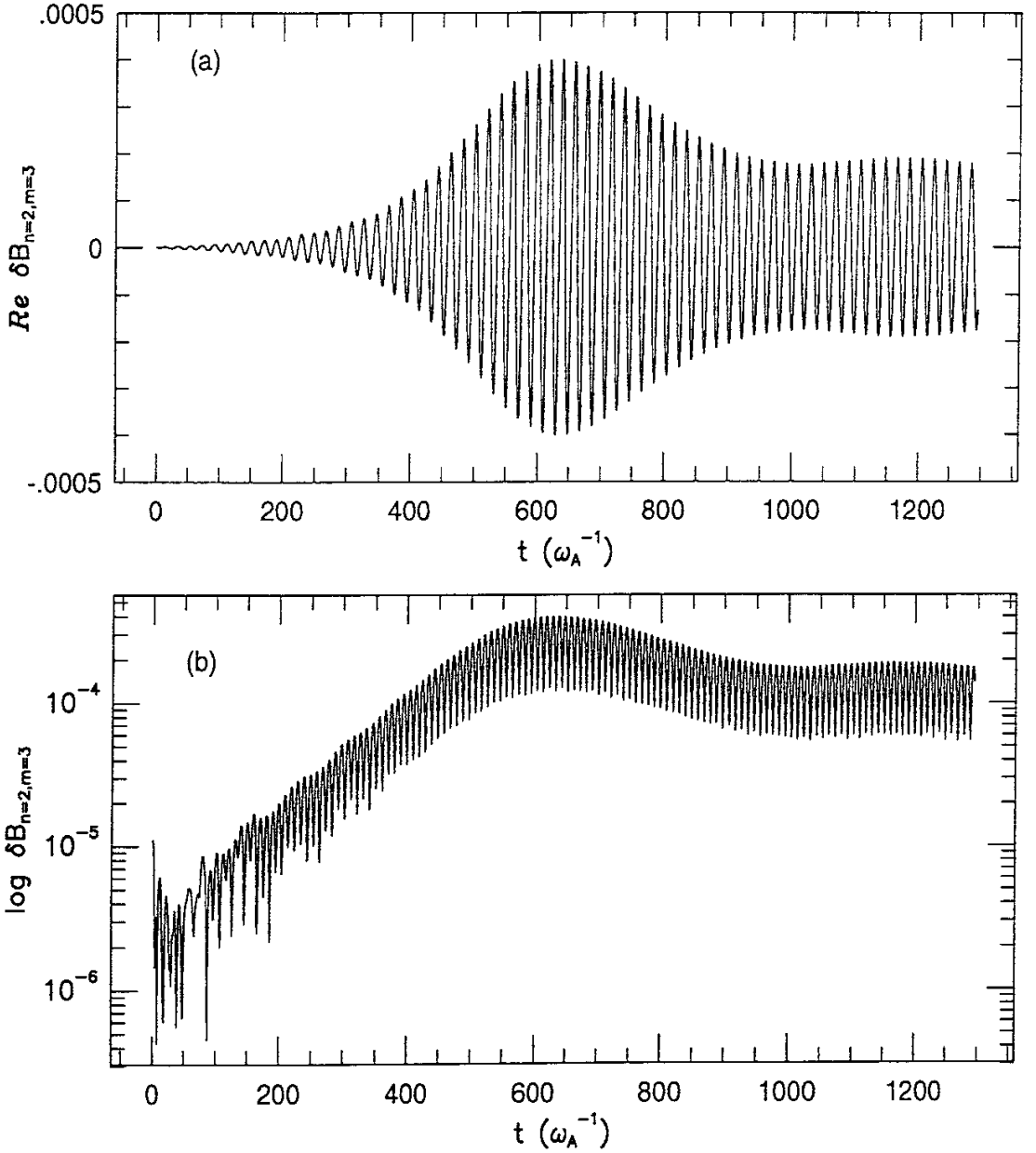
.0005
(a)
Re δB_{n=2,m=3}
0
-.0005
0
200
400
600
800
1000
1200
t (ω_A^{-1})
(b)
log δB_{n=2,m=3}
10^{-4}
10^{-5}
10^{-6}
0
200
400
600
800
1000
1200
t (ω_A^{-1})

Fig. 3

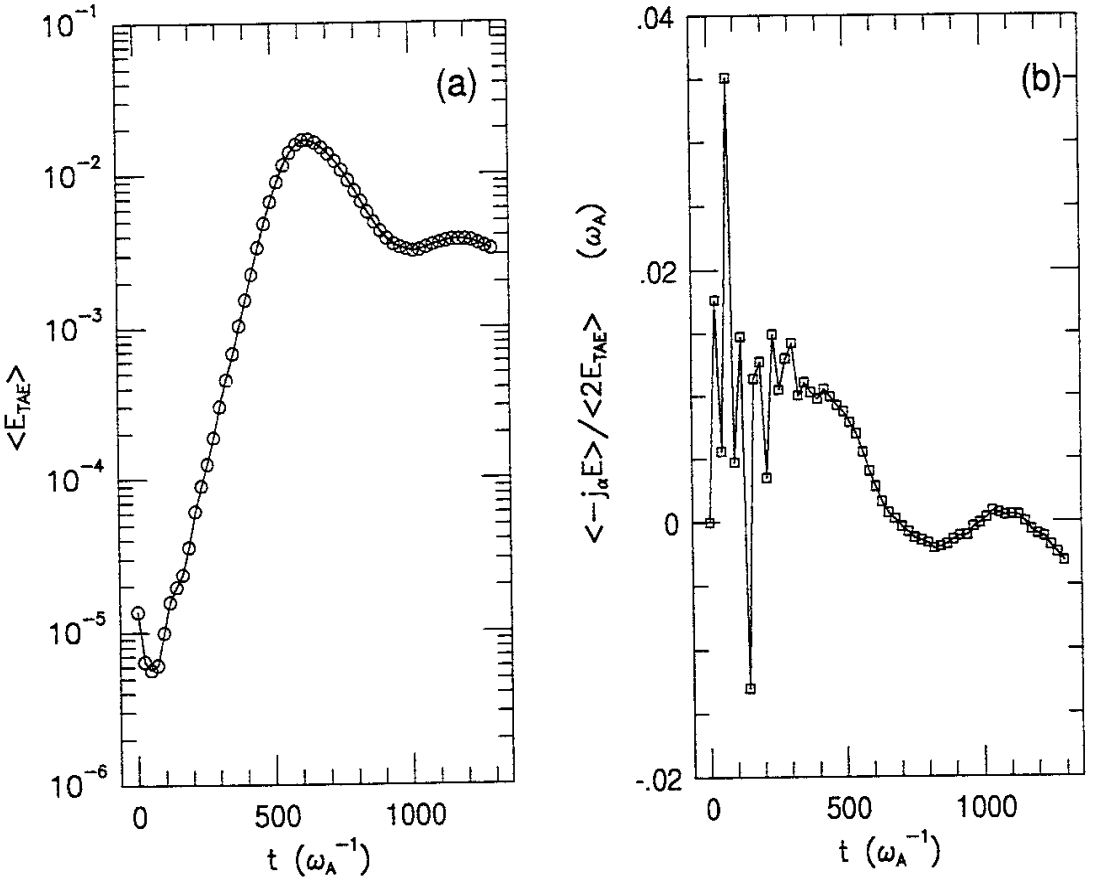
(a)
(b)
10^{-1}
10^{-2}
10^{-3}
10^{-4}
10^{-5}
10^{-6}
<E_{TAE}>
0
500
1000
t (ω_A^{-1})
.04
.02
0
-.02
<$-j_\alpha E$>/<$2E_{TAE}$> (ω_A)

Fig. 4

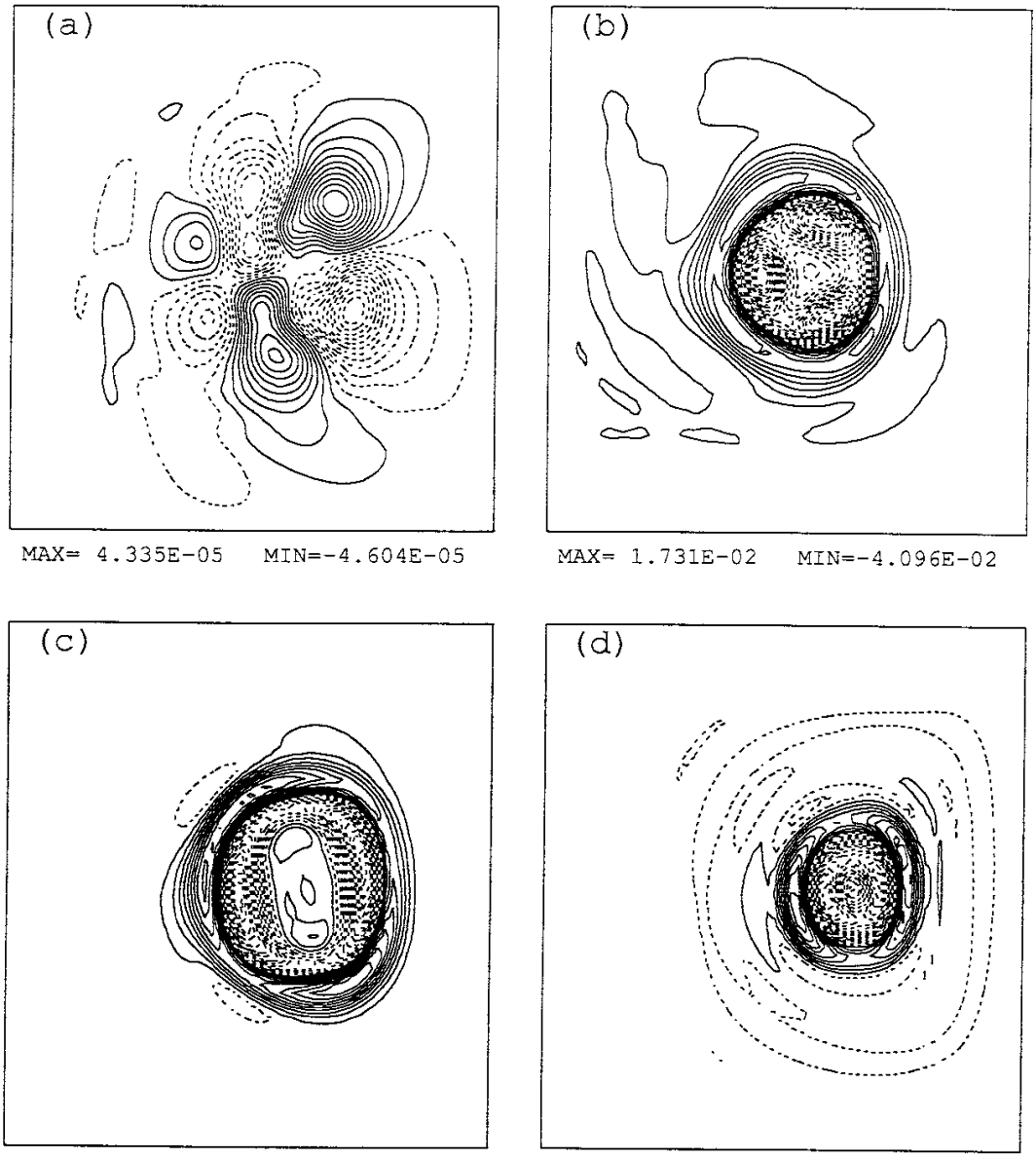
(a)
MAX= 4.335E-05 MIN=-4.604E-05
(b)
MAX= 1.731E-02 MIN=-4.096E-02
(c)
MAX= 1.115E-02 MIN=-1.732E-02
(d)
MAX= 8.967E-03 MIN=-1.297E-02

Fig. 5

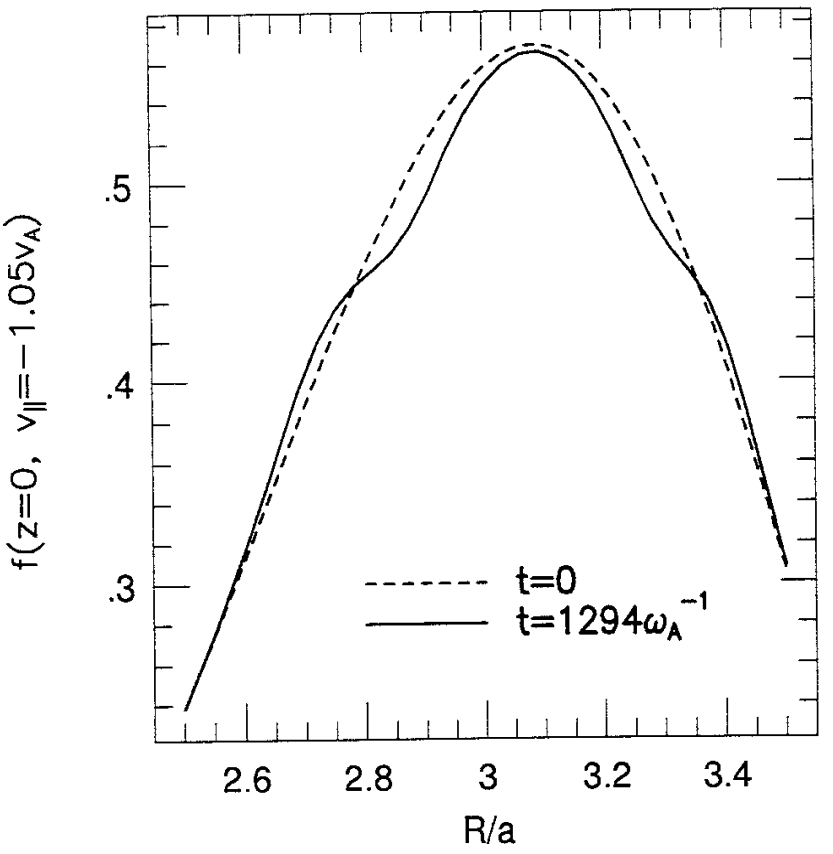

Fig. 6

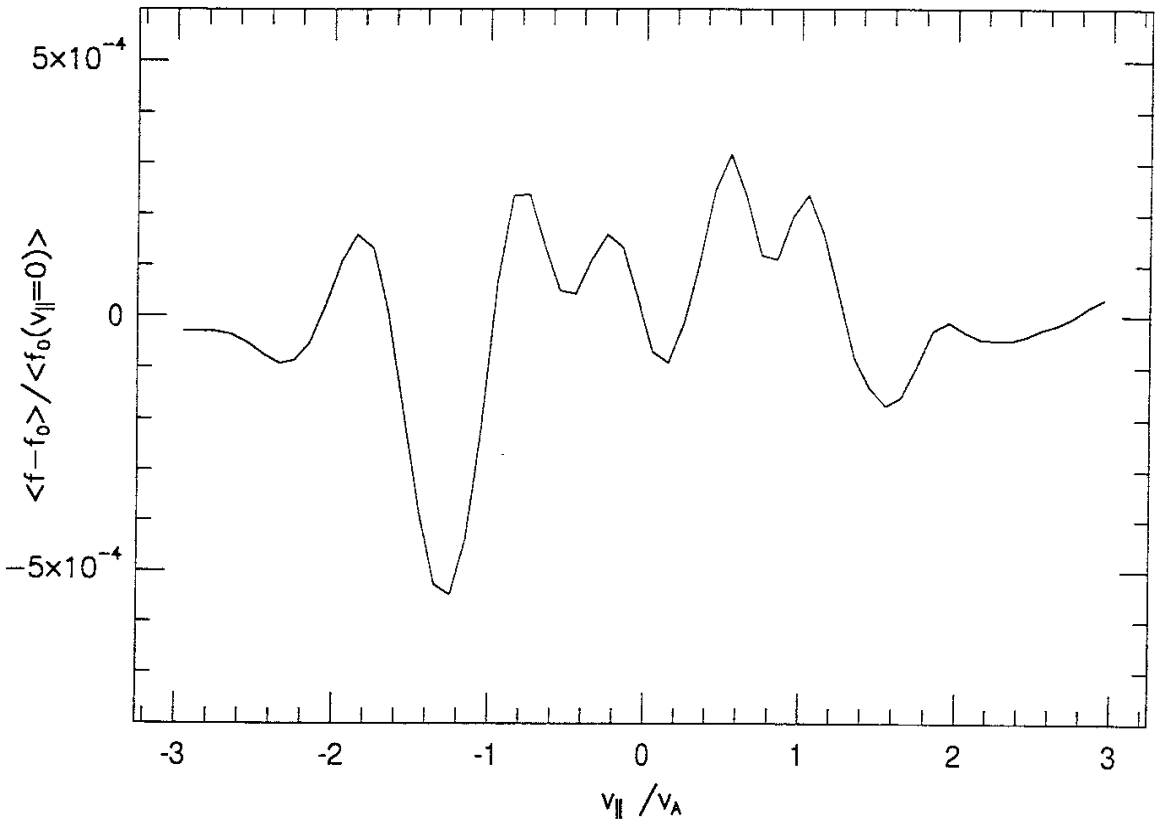

Fig. 7

Recent Issues of NIFS Series

NIFS-280 S. Okamura, K. Matsuoka, K. Nishimura, K. Tsumori, R. Akiyama, S. Sakakibara, H. Yamada, S. Morita, T. Morisaki,. N. Nakajima, K. Tanaka, J. Xu, K. Ida, H. Iguchi, A. Lazaros, T. Ozaki, H. Arimoto, A. Ejiri, M. Fujiwara, H. Idei. O. Kaneko, K. Kawahata, T. Kawamoto, A. Komori, S. Kubo, O. Motojima, V.D. Pustovitov, C. Takahashi, K. Toi and I. Yamada,
High-Beta Discharges with Neutral Beam Injection in CHS; Apr. 1994

NIFS-281 K. Kamada, H. Kinoshita and H. Takahashi,
Anomalous Heat Evolution of Deuteron Implanted Al on Electron Bombardment ; May 1994

NIFS-282 H. Takamaru, T. Sato, K. Watanabe and R. Horiuchi,
Super Ion Acoustic Double Layer; May 1994

NIFS-283 O.Mitarai and S. Sudo,
Ignition Characteristics in D-T Helical Reactors; June 1994

NIFS-284 R. Horiuchi and T. Sato,
Particle Simulation Study of Driven Magnetic Reconnection in a Collisionless Plasma; June 1994

NIFS-285 K.Y. Watanabe, N. Nakajima, M. Okamoto, K. Yamazaki, Y. Nakamura, M. Wakatani,
Effect of Collisionality and Radial Electric Field on Bootstrap Current in LHD (Large Helical Device); June 1994

NIFS-286 H. Sanuki, K. Itoh, J. Todoroki, K. Ida, H. Idei, H. Iguchi and H. Yamada,
Theoretical and Experimental Studies on Electric Field and Confinement in Helical Systems; June 1994

NIFS-287 K. Itoh and S-I. Itoh,
Influence of the Wall Material on the H-mode Performance; June 1994

NIFS-288 K. Itoh, A. Fukuyama, S.-I. Itoh, M. Yagi and M. Azumi,
Self-Sustained Magnetic Braiding in Toroidal Plasmas: July 1994

NIFS-289 Y. Nejoh,
Relativistic Effects on Large Amplitude Nonlinear Langmuir Waves in a Two-Fluid Plasma; July 1994

NIFS-290 N. Ohyabu, A. Komori, K. Akaishi, N. Inoue, Y. Kubota, A.I. Livshit, N. Noda, A. Sagara, H. Suzuki, T. Watanabe, O. Motojima, M. Fujiwara, A. Iiyoshi,
Innovative Divertor Concepts for LHD; July 1994

NIFS-291 H. Idei, K. Ida, H. Sanuki, S. Kubo, H. Yamada, H. Iguchi, S. Morita, S. Okamura, R. Akiyama, H. Arimoto, K. Matsuoka, K. Nishimura, K. Ohkubo, C. Takahashi, Y. Takita, K. Toi, K. Tsumori and I. Yamada, *Formation of Positive Radial Electric Field by Electron Cyclotron Heating in Compact Helical System*; July 1994

NIFS-292 N. Noda, A. Sagara, H. Yamada, Y. Kubota, N. Inoue, K. Akaishi, O. Motojima, K. Iwamoto, M. Hashiba, I. Fujita, T. Hino, T. Yamashina, K. Okazaki, J. Rice, M. Yamage, H. Toyoda and H. Sugai, *Boronization Study for Application to Large Helical Device*; July 1994

NIFS-293 Y. Ueda, T. Tanabe, V. Philipps, L. Könen, A. Pospieszczyk, U. Samm, B. Schweer, B. Unterberg, M. Wada, N. Hawkes and N. Noda, *Effects of Impurities Released from High Z Test Limiter on Plasma Performance in TEXTOR*; July. 1994

NIFS-294 K. Akaishi, Y. Kubota, K. Ezaki and O. Motojima, *Experimental Study on Scaling Law of Outgassing Rate with A Pumping Parameter*, Aug. 1994

NIFS-295 S. Bazdenkov, T. Sato, R. Horiuchi, K. Watanabe, *Magnetic Mirror Effect as a Trigger of Collisionless Magnetic Reconnection*, Aug. 1994

NIFS-296 K. Itoh, M. Yagi, S.-I. Itoh, A. Fukuyama, H. Sanuki, M. Azumi, *Anomalous Transport Theory for Toroidal Helical Plasmas*, Aug. 1994 (IAEA-CN-60/D-III-3)

NIFS-297 J. Yamamoto, O. Motojima, T. Mito, K. Takahata, N. Yanagi, S. Yamada, H. Chikaraishi, S. Imagawa, A. Iwamoto, H. Kaneko, A. Nishimura, S. Satoh, T. Satow, H. Tamura, S. Yamaguchi, K. Yamazaki, M. Fujiwara, A. Iiyoshi and LHD group, *New Evaluation Method of Superconductor Characteristics for Realizing the Large Helical Device;* Aug. 1994 (IAEA-CN-60/F-P-3)

NIFS-298 A. Komori, N. Ohyabu, T. Watanabe, H. Suzuki, A. Sagara, N. Noda, K. Akaishi, N. Inoue, Y. Kubota, O Motojima, M. Fujiwara and A. Iiyoshi, *Local Island Divertor Concept for LHD*; Aug. 1994 (IAEA-CN-60/F-P-4)

NIFS-299 K. Toi, T. Morisaki, S. Sakakibara, A. Ejiri, H. Yamada, S. Morita, K. Tanaka, N. Nakajima, S. Okamura, H. Iguchi, K. Ida, K. Tsumori, S. Ohdachi, K. Nishimura, K. Matsuoka, J. Xu, I. Yamada, T. Minami, K. Narihara, R. Akiyama, A. Ando, H. Arimoto, A. Fujisawa, M. Fujiwara, H. Idei, O. Kaneko, K. Kawahata, A. Komori, S. Kubo, R. Kumazawa, T. Ozaki, A. Sagara, C. Takahashi, Y. Takita and T. Watari, *Impact of Rotational-Transform Profile Control on Plasma Confinement and Stability in CHS*; Aug. 1994 (IAEA-CN-60/A6/C-P-3)

NIFS-300 H. Sugama and W. Horton,
Dynamical Model of Pressure-Gradient-Driven Turbulence and Shear Flow Generation in L-H Transition; Aug. 1994 (IAEA/CN-60/D-P-I-11)

NIFS-301 Y. Hamada, A. Nishizawa, Y. Kawasumi, K.N. Sato, H. Sakakita, R. Liang, K. Kawahata, A. Ejiri, K. Narihara, K. Sato, T. Seki, K. Toi, K. Itoh, H. Iguchi, A. Fujisawa, K. Adachi, S. Hidekuma, S. Hirokura, K. Ida, M. Kojima, J. Koog, R. Kumazawa, H. Kuramoto, T. Minami, I. Negi, S. Ohdachi, M. Sasao, T. Tsuzuki, J. Xu, I. Yamada, T. Watari,
Study of Turbulence and Plasma Potential in JIPP T-IIU Tokamak; Aug. 1994 (IAEA/CN-60/A-2-III-5)

NIFS-302 K. Nishimura, R. Kumazawa, T. Mutoh, T. Watari, T. Seki, A. Ando, S. Masuda, F. Shinpo, S. Murakami, S. Okamura, H. Yamada, K. Matsuoka, S. Morita, T. Ozaki, K. Ida, H. Iguchi, I. Yamada, A. Ejiri, H. Idei, S. Muto, K. Tanaka, J. Xu, R. Akiyama, H. Arimoto, M. Isobe, M. Iwase, O. Kaneko, S. Kubo, T. Kawamoto, A. Lazaros, T. Morisaki, S. Sakakibara, Y. Takita, C. Takahashi and K. Tsumori,
ICRF Heating in CHS; Sep. 1994 (IAEA-CN-60/A-6-I-4)

NIFS-303 S. Okamura, K. Matsuoka, K. Nishimura, K. Tsumori, R. Akiyama, S. Sakakibara, H. Yamada, S. Morita, T. Morisaki, N. Nakajima, K. Tanaka, J. Xu, K. Ida, H. Iguchi, A. Lazaros, T. Ozaki, H. Arimoto, A. Ejiri, M. Fujiwara, H. Idei, A. Iiyoshi, O, Kaneko, K. Kawahata, T. Kawamoto, S. Kubo, T. Kuroda, O. Motojima, V.D. Pustovitov, A. Sagara, C. Takahashi, K. Toi and I. Yamada,
High Beta Experiments in CHS; Sep. 1994 (IAEA-CN-60/A-2-IV-3)

NIFS-304 K. Ida, H. Idei, H. Sanuki, K. Itoh, J. Xu, S. Hidekuma, K. Kondo, A. Sahara, H. Zushi, S.-I. Itoh, A. Fukuyama, K. Adati, R. Akiyama, S. Bessho, A. Ejiri, A. Fujisawa, M. Fujiwara, Y. Hamada, S. Hirokura, H. Iguchi, O. Kaneko, K. Kawahata, Y. Kawasumi, M. Kojima, S. Kubo, H. Kuramoto, A. Lazaros, R. Liang, K. Matsuoka, T. Minami, T. Mizuuchi, T. Morisaki, S. Morita, K. Nagasaki, K. Narihara, K. Nishimura, A. Nishizawa, T. Obiki, H. Okada, S. Okamura, T. Ozaki, S. Sakakibara, H. Sakakita, A. Sagara, F. Sano, M. Sasao, K. Sato, K.N. Sato, T. Saeki, S. Sudo, C. Takahashi, K. Tanaka, K. Tsumori, H.Yamada, I. Yamada, Y. Takita, T. Tuzuki, K. Toi and T. Watari,
Control of Radial Electric Field in Torus Plasma; Sep. 1994 (IAEA-CN-60/A-2-IV-2)

NIFS-305 T. Hayashi, T. Sato, N. Nakajima, K. Ichiguchi, P. Merkel, J. Nührenberg, U. Schwenn, H. Gardner, A. Bhattacharjee and C.C.Hegna,
Behavior of Magnetic Islands in 3D MHD Equilibria of Helical Devices; Sep. 1994 (IAEA-CN-60/D-2-II-4)

NIFS-306 S. Murakami, M. Okamoto, N. Nakajima, K.Y. Watanabe, T. Watari, T. Mutoh, R. Kumazawa and T. Seki,

Monte Carlo Simulation for ICRF Heating in Heliotron/Torsatrons; Sep. 1994 (IAEA-CN-60/D-P-I-14)

NIFS-307 Y. Takeiri, A. Ando, O. Kaneko, Y. Oka, K. Tsumori, R. Akiyama, E. Asano, T. Kawamoto, T. Kuroda, M. Tanaka and H. Kawakami,
Development of an Intense Negative Hydrogen Ion Source with a Wide-Range of External Magnetic Filter Field; Sep. 1994

NIFS-308 T. Hayashi, T. Sato, H.J. Gardner and J.D. Meiss,
Evolution of Magnetic Islands in a Heliac; Sep. 1994

NIFS-309 H. Amo, T. Sato and A. Kageyama,
Intermittent Energy Bursts and Recurrent Topological Change of a Twisting Magnetic Flux Tube; Sep.1994

NIFS-310 T. Yamagishi and H. Sanuki,
Effect of Anomalous Plasma Transport on Radial Electric Field in Torsatron/Heliotron; Sep. 1994

NIFS-311 K. Watanabe, T. Sato and Y. Nakayama,
Current-profile Flattening and Hot Core Shift due to the Nonlinear Development of Resistive Kink Mode; Oct. 1994

NIFS-312 M. Salimullah, B. Dasgupta, K. Watanabe and T. Sato,
Modification and Damping of Alfvén Waves in a Magnetized Dusty Plasma; Oct. 1994

NIFS-313 K. Ida, Y. Miura, S -I. Itoh, J.V. Hofmann, A. Fukuyama, S. Hidekuma, H. Sanuki, H. Idei, H. Yamada, H. Iguchi, K. Itoh,
Physical Mechanism Determining the Radial Electric Field and its Radial Structure in a Toroidal Plasma; Oct. 1994

NIFS-314 Shao-ping Zhu, R. Horiuchi, T. Sato and The Complexity Simulation Group,
Non-Taylor Magnetohydrodynamic Self-Organization; Oct. 1994

NIFS-315 M. Tanaka,
Collisionless Magnetic Reconnection Associated with Coalescence of Flux Bundles; Nov. 1994

NIFS-316 M. Tanaka,
Macro-EM Particle Simulation Method and A Study of Collisionless Magnetic Reconnection; Nov. 1994

NIFS-317 A. Fujisawa, H. Iguchi, M. Sasao and Y. Hamada,
Second Order Focusing Property of 210° Cylindrical Energy Analyzer; Nov. 1994

NIFS-318 T. Sato and Complexity Simulation Group,
Complexity in Plasma - A Grand View of Self- Organization; Nov. 1994